Stress dependence of the zone-center optical phonons of LaF_3

F. Cerdeira, V. Lemos, and R. S. Katiyar
Instituto de Física, Universidade Estadual de Campinas, 13.100 Campinas, S.P., Brasil
(Received 20 September 1978)

The Raman spectrum of LaF_3 was studied both with and without uniaxial stress. Spectra of unstressed samples taken at room temperature and also at 77 and 2.2 K allow identification of all observed structure, thereby correcting some inaccurate assignments in previously published works. Most of the Raman lines were studied under uniaxial stress at 77 K. This study allows the determination of anharmonic coefficients important in the lattice-dynamical description of the material. Also, the stress dependence of twofold degenerate modes permits the distinguishing between the two proposed point-group symmetries, D_{6h} and D_{3d}, for the unit cell of LaF_3. Thus quantitative comparison between the splittings produced in these modes by forces applied along two well-chosen crystallographic directions establishes that the correct point-group symmetry is D_{3d}.

I. INTRODUCTION

The crystal structure of LaF_3 has been the subject of several conflicting studies,[1-10] which are briefly reviewed in the Raman work of Bauman and Porto.[11] The two most probable structures emerging from these studies have hexamolecular unit cells belonging to space groups D^3_{6h} and D^4_{3d}, respectively. Analysis of the Raman and infrared spectrum[11] favor the designation of D^4_{3d} for the space group of LaF_3, while indicating that the deviations from the more symmetrical D^3_{6h} structure are small. A more recent study[12] of the Raman spectrum of LaF_3 confirms this conclusion, although changing some of the identifications of the structure in the Raman spectrum made by Bauman and Porto.[11] In the present work we study the changes in the Raman spectrum of LaF_3 introduced by the application of high uniaxial stress. These changes are well described by first-order perturbation theory using an effective strain Hamiltonian which has been successfully applied to a wide variety of materials.[13-18] The behavior of the difference zone-center optical modes under stress directed along different crystallographic directions is used to characterize the point-group symmetry of the crystal. In particular, comparison of the splitting produced in two fold degenerate modes by forces directed along the $[0\bar{1}10]$ crystallographic direction and along an axis at 45° between the optic axis (z) and the xy plane, respectively, establish the point-group symmetry of LaF_3 as being D_{3d}. Also the data are used to obtain deformation potential constants for most of the Raman active modes of this crystal. These anharmonic constants are of great importance in the lattice-dynamical description of any solid.

II. EXPERIMENTAL PROCEDURE

Zero-pressure Raman spectra of LaF_3 were taken at room temperature and also at 77 and 2.2 K with the sample immersed in liquid nitrogen or superfluid helium, respectively. Uniaxial stress measurements were performed at 77 K with sample and stress frame immersed in liquid nitrogen contained in a long cylindrical glass Dewar. We used 1W of the 5145- and 4880-Å lines of an argon ion laser as exciting radiation. The scattered light was analyzed with a SPEX double monochromator with standard cooled photomultiplier plus electrometer detection. The Rayleigh line, taken with a neutral density filter, was used as calibration to determine line positions. Instrumental width was kept below 1 cm^{-1}.

The samples were oriented to ±1° and cut from a single crystal obtained commercially[19] into parallelepipeds of dimensions ~3×2×2 mm, the long dimension being the direction of the compression. End planes to be pressed were polished parallel. The samples were glued onto brass cups polished flat. The stress apparatus is described elsewhere.[20] The different configurations used are referred to a set of mutually orthogonal axes x, y, z, with the z axis taken to coincide with the optic (hexagonal or trigonal) axis, x chosen parallel to one of the two fold axis of the D_{3d} point group and y chosen perpendicular to both x and z in order to form a right-handed Cartesian system. Two cuts were used in our experiments: one with the parallelepiped faces perpendicular to the $\hat{x}$, $\hat{y}$, and $\hat{z}$ directions and another with the faces perpendicular to a new set of axes, x', y', z' defined by

TABLE I. Number (N) and symmetry type of expected Raman-active modes for both proposed structures of LaF_3, and useful sets of basis functions for each irreducible representation.

(a) Space group D_{6h}^3			(b) Space group D_{3d}^4		
Representation	N	Basis functions	Representation	N	Basis functions
A_{1g}	3	$f_0 = X^2 + Y^2; Z^2$	A_{1g}	5	$f_0 = X^2 + Y^2; Z^2$
E_{1g}	4	$f_\alpha^{(1)} = YZ$ $f_\beta^{(1)} = -XZ$	E_g	12	$f_\alpha = YZ; X^2 - Y^2$ $f_\beta = -XZ; -2XY$
E_{2g}	8	$f_\alpha^{(2)} = X^2 - Y^2$ $\quad f_\alpha^{(2)\prime} = f_\alpha^{(2)2} - f_\beta^{(2)2}$ $f^{(2)} = -2XY$ $\quad f_\beta^{(2)\prime} = -2f_\alpha^{(2)} f_\beta^{(2)}$			

$$\hat{x}' = \hat{x}\,,$$
$$\hat{y}' = (1/\sqrt{2})(\hat{y} + \hat{z})\,, \qquad (1)$$
$$\hat{z}' = (1/\sqrt{2})(-\hat{y} + \hat{z})\,.$$

Spectra were taken with the applied force directed along the $\hat{x}$ and $\hat{z}'$ directions, respectively. Some spectra were taken with $\hat{F} /\!/ \hat{z}$, although only qualitative conclusions could be drawn from these results, since in this case the sample cleaved at pressures below 1 kbar. The scattering configuration is specified by standard notation[21] of the form $x(zx)y$, in which the first and last letters indicate the direction of propagation of incident and scattered light, respectively, and the first and second letters in parenthesis indicate their respective polarization.

III. THEORY

The number and symmetry type of expected Raman-active modes for both proposed structures[11] of LaF_3, together with useful basis functions for each irreducible representation,[22] is given

TABLE II. Polarizability tensors of the Raman-active modes of LaF_3 for each of the two proposed structures for both cuts used in our experiment.

(a) Point group D_{6h} Polarizability tensor			(b) Point group D_{3d} Polarizability tensor		
Symmetry	$x\,y\,z$ cut	x', y', z' cut	Symmetry	$x\,y\,z$ cut	$x'\,y'\,z'$ cut
A_{1g}	$\begin{bmatrix} p & 0 & 0 \\ 0 & p & 0 \\ 0 & 0 & q \end{bmatrix}$	$\begin{bmatrix} p & 0 & 0 \\ 0 & \frac{1}{2}(p+q) & \frac{1}{2}(q-p) \\ 0 & \frac{1}{2}(q-p) & \frac{1}{2}(q+p) \end{bmatrix}$	A_{1g}	$\begin{bmatrix} p & 0 & 0 \\ 0 & p & 0 \\ 0 & 0 & q \end{bmatrix}$	$\begin{bmatrix} p & 0 & 0 \\ 0 & \frac{1}{2}(p+q) & \frac{1}{2}(q-p) \\ 0 & \frac{1}{2}(q+p) & \frac{1}{2}(p+q) \end{bmatrix}$
E_{1g} (α)	$\begin{bmatrix} 0 & 0 & 0 \\ 0 & 0 & s \\ 0 & s & 0 \end{bmatrix}$	$\begin{bmatrix} 0 & 0 & 0 \\ 0 & s & 0 \\ 0 & 0 & -s \end{bmatrix}$	E_g (α)	$\begin{bmatrix} r & 0 & 0 \\ 0 & -r & s \\ 0 & s & 0 \end{bmatrix}$	$\begin{bmatrix} r & 0 & 0 \\ 0 & s-\frac{1}{2}r & \frac{1}{2}r \\ 0 & \frac{1}{2}r & -s-\frac{1}{2}r \end{bmatrix}$
E_{1g} (s)	$\begin{bmatrix} 0 & 0 & -s \\ 0 & 0 & 0 \\ -s & 0 & 0 \end{bmatrix}$	$\begin{bmatrix} 0 & -s/\sqrt{2} & -s/\sqrt{2} \\ -s/\sqrt{2} & 0 & 0 \\ -s/\sqrt{2} & 0 & 0 \end{bmatrix}$	E_g	$\begin{bmatrix} 0 & -r & -s \\ -s & 0 & 0 \\ -s & 0 & 0 \end{bmatrix}$	$\begin{bmatrix} 0 & \frac{-(r+s)}{\sqrt{2}} & \frac{r-s}{\sqrt{2}} \\ \frac{-(r+s)}{\sqrt{2}} & 0 & 0 \\ \frac{r-s}{\sqrt{2}} & 0 & 0 \end{bmatrix}$
E_{2g} (α)	$\begin{bmatrix} r & 0 & 0 \\ 0 & -r & 0 \\ 0 & 0 & 0 \end{bmatrix}$	$\begin{bmatrix} r & 0 & 0 \\ 0 & -\frac{1}{2}r & \frac{1}{2}r \\ 0 & \frac{1}{2}r & -\frac{1}{2}r \end{bmatrix}$			
E_{2g} (s)	$\begin{bmatrix} 0 & -r & 0 \\ -r & 0 & 0 \\ 0 & 0 & 0 \end{bmatrix}$	$\begin{bmatrix} 0 & -r/\sqrt{2} & r/\sqrt{2} \\ -r/\sqrt{2} & 0 & 0 \\ r/\sqrt{2} & 0 & 0 \end{bmatrix}$			

in Table I. Table II lists the polarizability tensor for each type of mode for both cuts used in our experiment. In both these Tables first and second rows of two-dimensional irreducible representations are labeled α and β, respectively, in such a way as to correspond to the X and Y components of the E representation of point group D_3, which is a subgroup of both proposed point groups (D_{6h} and D_{3d}). This labeling of partner functions, or polarizability tensors, has the advantage of allowing us to think of these phonons as vibrating "parallel" or "perpendicular" to the applied force, a concept which, although not strictly meaningful in this case, permits quick rule-of-thumb derivation of selection rules.

Under uniaxial stress the crystal symmetry is reduced. The symmetry of the deformed crystal is determined by the elements common to both the unstrained crystal and the strain ellipsoid. Thus a compressive force directed along the optic axis leaves the crystal symmetry unaltered, whereas forces directed along other crystallographic directions change the point-group symmetry in the manner indicated in Table III. To the extent that the observed effects depend linearly on the applied force, the splittings and shifts of the Raman lines under uniaxial stress are well described in first-order perturbation theory using an effective strain Hamiltonian dependent upon a number of constant parameters called deformation potentials.[16-18] For either of the two proposed point groups (D_{3d} or D_{6h}), this theory predicts for the frequency shifts of A_{1g} modes[16,17]:

$$\Delta\omega_{A_{1g}} = a(\epsilon_{xx}+\epsilon_{yy}) + b\epsilon_{zz}\,, \tag{2}$$

where a and b are deformation potential constants and ϵ_{ij} are the components of the strain tensor. Doubly degenerate E modes behave differently under stress depending upon whether the point group is D_{3d} or D_{6h}. In this case we have[16,17]

$$\Delta\omega_E = a(\epsilon_{xx}+\epsilon_{yy}) + b\epsilon_{zz} \pm \tfrac{1}{2}\delta\omega\,, \tag{3}$$

where

$$\delta\omega = 2\{[c(\epsilon_{xx}-\epsilon_{yy}) + d\epsilon_{yz}]^2 + [2c\epsilon_{xy} + d\epsilon_{xz}]^2\}^{1/2}\,, \tag{4}$$

for D_{3d} (in which case $E = E_g$), and

$$\delta\omega = 2c[(\epsilon_{xx}-\epsilon_{yy})^2 + 4\epsilon_{xy}^2]^{1/2} \tag{5}$$

for D_{6h}. In this last case the shifts and splittings of E_{1g} and E_{2g} modes have identical expressions, although, of course, the numerical values of the deformation potential constants vary from mode to mode. In the analysis of experimental data it is more convenient to express Eqs. (3)–(5) in terms of the components of the stress tensor $\sigma_{ij} = T(\hat{F}\cdot\hat{i})(\hat{F}\cdot\hat{j})$, where $\hat{i}$ and $\hat{j}$ are Cartesian axes, as defined in Nye,[23] $\hat{F}$ is a unit vector in the direction of the applied force, and T is the compressive force per unit area. Using the standard strain-stress relationships,[23] we obtain for the D_{3d} point group[16]

$$\Delta\omega_{A_{1g}} = a'(\sigma_{xx}+\sigma_{yy}) + b'\sigma_{zz}\,, \tag{6}$$

$$\Delta\omega_{E_g} = a'(\sigma_{xx}+\sigma_{yy}) + b'\sigma_{zz} \pm \tfrac{1}{2}\delta\omega\,, \tag{7}$$

$$\delta\omega = 2\{[c'(\sigma_{xx}-\sigma_{yy}) + d'\sigma_{yz}]^2 + [2c'\sigma_{xy} + d'\sigma_{xz}]^2\}^{1/2}\,, \tag{8}$$

with

$$a' = a(S_{11}+S_{12}) + bS_{13},\quad c' = c(S_{11}-S_{12}) + \tfrac{1}{2}dS_{14}\,, \tag{9}$$

$$b' = 2aS_{13} + bS_{33},\quad d' = 2cS_{14} + \tfrac{1}{2}dS_{44}\,,$$

where the S_{ij}'s are the elastic compliances. Similarly, for the D_{6h} point group we obtain[17]

$$\Delta\omega_{A_{1g}} = a'(\sigma_{xx}+\sigma_{yy}) + b'\sigma_{zz}\,, \tag{10}$$

$$\Delta\omega_{E_{1g}} = \Delta\omega_{E_{2g}} = a'(\sigma_{xx}+\sigma_{yy}) + b'\sigma_{zz} \pm \tfrac{1}{2}\delta\omega\,, \tag{11}$$

$$\delta\omega = 2c'[(\sigma_{xx}-\sigma_{yy})^2 + 4\sigma_{xy}^2]^{1/2}\,, \tag{12}$$

where

$$a' = a(S_{11}+S_{12}) + bS_{13},\quad c' = c(S_{11}-S_{12})\,,$$
$$b' = 2aS_{13} + bS_{33}\,. \tag{13}$$

The frequency changes and eigenfunctions characterizing the two stress-induced components of the E lines for various force directions are listed in Table III. Notice that the two eigenmodes of E symmetry for forces directed along the $\hat{x}$, $\hat{y}$, or $\hat{z}'$ directions are the α and β components of Tables I and II. Thus the polarization characteristics of this eigenmodes can be obtained with the polarizability tensors of Table II, and we can choose polarizations which allow one of the components while excluding the other, thus facilitating the determination of the frequency shifts and splittings.

The above discussion shows that the difference between the stress behavior of crystals with D_{6h} or D_{3d} point-group symmetry resides in the existence of an additional deformation potential constant d' necessary to describe the splitting of E modes in the latter case. Thus for a crystal of point group D_{6h} the splitting $\delta\omega$ of E modes for $\hat{F}\|\hat{z}'$ is exactly half of the splitting obtained for $\hat{F}\|\hat{x}$ (see Table III). This is not the case when the point group of the crystal is D_{3d}, due to the existence of the additional deformation-potential constant d' (see Table III). Hence measurement of the splittings of the various E modes for these two directions of applied force should serve to determine whether the point-group symmetry of LaF_3 is D_{3d} or D_{6h}. In fact, the ratio d'/c' constitutes a measure of the deviations from the more symmetric D_{6h} structure.

TABLE III. Eigenvalues and eigenfunctions for doubly degenerate modes under uniaxial stress for both proposed point-group symmetries of LaF_3. Here f_α refers either to basis functions of D_{6h} or D_{3d} as listed in Table II.

Force direction	Symmetry $T=0$ $T\neq0$	Eigenvalues [a]	Symmetry $T=0$ $T\neq0$	Eigenvalues [a]	Eigenfunctions [b]
$\hat{F}//\hat{z}$	D_{6h} D_{6h}	$b'T$ $b'T$	D_{3d} D_{3d}	$b'T$ $b'T$	Any linear combination of f_α and f_β
$F//\hat{x}$	D_{6h} D_{2h}	$(a'+c')T$ $(a'-c')T$	D_{3d} C_{2h}	$(a'+c')T$ $(a'-c')T$	f_α f_β
$F//\hat{z}'$	D_{6h} C_{2h}	$\frac{1}{2}(a'+b'-c')T$ $\frac{1}{2}(a'+b'+c')T$	D_{3d} C_{2h}	$\frac{1}{2}(a'+b'-c'-d')T$ $\frac{1}{2}(a'+b'+c'+d')T$	f_α f_β
Arbitrary	D_{6h} C_i	$a'(\sigma_{xx}+\sigma_{yy})+b'\sigma_{zz}+\frac{1}{2}\delta\omega$ $a'(\sigma_{xx}+\sigma_{yy})+b'\sigma_{zz}-\frac{1}{2}\delta\omega$ $\delta\omega=2c'(\sigma_{xx}-\sigma_{yy})^2+4\sigma_{xy}^2{}^{1/2}$	D_{3d} C_i	$a'(\sigma_{xx}+\sigma_{yy})+b'\sigma_{zz}+\frac{1}{2}\delta\omega$ $a'(\sigma_{xx}+\sigma_{yy})+b'\sigma_{zz}-\frac{1}{2}\delta\omega$ $\delta\omega=2\{[\sigma'(\sigma_{xx}-\sigma_{yy})+d'\sigma_{yz}]^2+$ $+(2c'\sigma_{xy}+d'\sigma_{xz})^2\}^{1/2}$	$\Psi_1=f_\alpha\cos\Omega/2+f_\beta\sin\Omega/2)$ $\Psi_2=-f_\alpha\sin\Omega/2+f_\beta\cos\Omega/2)$

[a] $\sigma_{ij}=T(\hat{F}\cdot\hat{i})(\hat{F}\cdot\hat{j})$, where T is the force per unit area.

[b] Here $\cos(\Omega)=2[c'(\sigma_{xx}-\sigma_{yy})+d'\sigma_{yz}]/\delta\omega$ and $\sin\Omega=2(2c'\sigma_{xy}+d'\sigma_{xz})/\delta\omega$ for D_{3d}, and the same for D_{6h} setting $d'=0$.

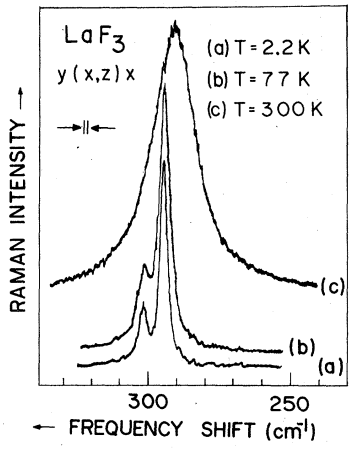

FIG. 1. Composite structure of the peak identified in Ref. 11 as E_{1g} (290) brought out by lower temperature and higher resolution.

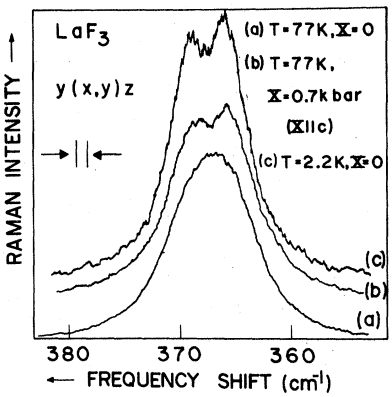

FIG. 2. Composite structure of the peak identified in Ref. 11 as E_{2g} (366) brought out by a uniaxial stress along the optical axis or liquid-helium temperature.

IV. RESULTS AND DISCUSSION

We studied in detail the zero-stress Raman spectrum of LaF_3 at room, liquid-nitrogen, and superfluid-liquid-helium temperatures. Our results show some differences from the previously reported Raman work of Bauman and Porto.[11] We found that two structures identified by these authors as single peaks, E_{1g} (290 cm^{-1}) and E_{2g} (366 cm^{-1}), using the notation of the D_{6h} point group, are really double peaks. The composite structure of the former peak is revealed using better resolution both at 77 and 2.2 K, as shown in Fig. 1. The frequency values (here in units of wave number, cm^{-1}) for the two resulting peaks are listed in Table IV. The structure identified in Ref. 11 as one peak obeying E_{2g} selection rules located at $\omega = 366$ cm^{-1} resolves into two peaks of the same symmetry by either lowering the temperature to 2.2 K or by applying a small uniaxial stress along the optic axis at 77 K, as shown in Fig. 2. Also, we disagree with some of the other assignments in Ref. 11. The peaks identified there as A_{1g}

TABLE IV. Designation of Raman peaks in LaF_3.

Symmetry		Ref. 11	Our Work	Frequency in cm^{-1} Our work
D_{3d}	D_{6h}	70 K	77 K	2.2 K
		120	119.4	119.4
		231	228.6	229.7
A_{1g}	A_{1g}	283	Not found	
		305	305.0	305.0
		390	389.4	390.1
		145	144.6	145.8
		203	202.0	202.5
	E_{1g}	226	225.0	225.8
		290	292.7	293.5
			299.4	300.8
E_g				
		79	77.6	77.6
		145	Spillover from E_{1g}	
		163	163.1	163.2
		281?	Not found	
	E_{2g}	301	Spillover from E_{1g}	
		315	314.0	314.4
		325	Not found	
		366	365	365.1
				368.3

(283 cm^{-1}), E_{2g} (281 cm^{-1}), and E_{2g} (325 cm^{-1}) do not appear in our spectra under any conditions of resolution or enlargement of scale. We further believe that the structure identified in Ref. 11 as E_{2g} (145 cm^{-1}) is a spillover from the observed E_{1g} peak at the same frequency. This is consistent with relative intensity considerations and with the fact that these structures coincide exactly in frequency for all temperatures measured and for all values and directions of pressure at constant temperature. Hence we conclude that there exists only one peak at $\omega = 144.6$ cm^{-1} ($T = 77$ K) which approximately obeys E_{1g} selection rules with a slight E_{2g} character also, i.e., its polarizability tensor corresponds to those listed in Table II (b) having $|s| \gg |r|$. The same arguments apply to the structure identified in Ref. 11 as E_{2g} (301 cm^{-1}) which we believe to be the same as the peak obeying E_{1g} selection rules found by us to lie at $\omega = 300.8$ cm^{-1} ($T = 77$ K). This confusion could have originated from the fact that this structure is one of the members of a doublet (see Fig. 1) identified as a single peak in the spectra of Ref. 11. In Table IV we list the correct designation of all the structures observed in our Raman spectra together with those of Ref. 11 for comparison purposes. We found a total of four A_{1g}, five E_{1g}, and five E_{2g} peaks. Since the D_{6h}^3 structure requires the existence of only three A_{1g} and four E_{1g} peaks (see Table I), our findings support the D_{3d}^4 structure. This conclusion is further reinforced by the above-mentioned fact that some of the peaks of E_{1g} symmetry appear residually in the spectra where only E_{2g} peaks are allowed. In this case, one A_{1g} and two E_g peaks remain to be found.

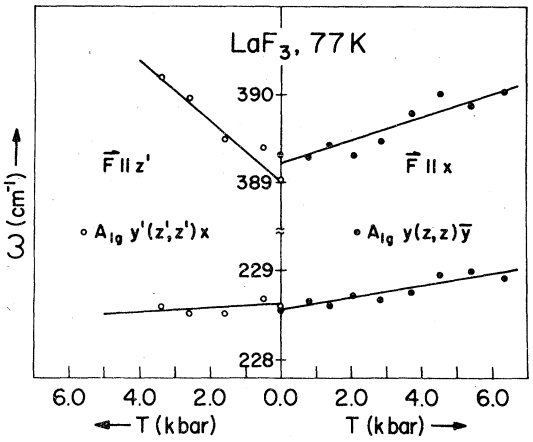

FIG. 3. Frequency vs stress for representative A_{1g} modes in LaF_3 for two directions of the applied force.

Having completed the identification of the structures appearing in the Raman spectrum of LaF_3, we proceed to discuss the behavior of these peaks under uniaxial stress applied along two different crystallographic directions: those designated by $\hat{x}$ and $\hat{z}'$ in Sec. II. We selected some representative peaks of each symmetry for quantitative study. In what follows we describe the effect of pressure for each symmetry type separately, referring to each peak by its D_{6h} symmetry followed by its frequency value (in parenthesis) at 77 K, rounded off to the nearest integer.

TABLE V. Deformation-potential constants for the Raman-active phonons of LaF_3. The experimental uncertainties are indicated in parentheses below the numerial value of each parameter.

Mode	Deformation potentials in cm^{-1}/kbar a'	b'	c'	d'	d'/c'
A_{1g} (229)	0.07 (±0.01)	−0.11 (±0.05)	...	...	...
A_{1g} (389)	0.13 (±0.02)	0.51 (±0.08)	...	...	...
E_{2g} (78)	0.05 (±0.01)	−0.05 (±0.05)	0.13 (±0.01)	0.03 (±0.06)	0.2 (±0.05)
E_{2g} (314)	0.42 (±0.02)	−0.21 (±0.06)	0.21 (±0.02)	−0.14 (±0.08)	−0.7 (±0.5)
E_{1g} (145)	0.16 (±0.01)	−0.11 (±0.05)	0.13 (±0.01)	0.11 (±0.06)	0.8 (±0.5)
E_{1g} (202)	0.02 (±0.01)	0.11 (±0.06)	−0.11 (±0.01)	0.02 (±0.07)	−0.2 (±0.6)
E_{1g} (293)	0.12 (±0.01)	0.03 (±0.06)	−0.21 (±0.01)	0.32 (±0.07)	−1.5 (±0.4)
E_{1g} (299)	0.32 (±0.02)	−0.10 (±0.09)	0.08 (±0.02)	−0.35 (±0.11)	−4.4 (±2.5)

A. A_{1g} lines

The strongest peak in the Raman spectrum obeying A_{1g} selection rules were those located at 228.6 and 389.4 cm^{-1} at 77 K. The remaining two lines were weaker and showed small shifts under uniaxial stress, thus making quantitative analysis difficult. In the x,y,z cut the strongest signals were obtained when both incident and scattered light were polarized along the z (optic) axis. Analogously best results were obtained in the x', y',z' cuts when both incident and scattered light were polarized along the z' axis. Hence the configuration used for experiments where $\hat{F}\|\hat{x}$ was $y(zz)\bar{y}$ and for $\hat{F}\|\hat{z}'$, $y'(z'z')x$. Peak position as a function of applied stress is plotted in Fig. 3 for these two lines. In this figure full and open dots represent peak positions for $\hat{F}\|\hat{x}$ and $\hat{F}\|\hat{z}'$, respectively, while solid lines are linear least-squares fits to them. From the slopes of these lines and the expressions in Eqs. (6) or (10), the deformation potentials a' and b' are obtained. The resulting parameters are listed in Table V. Since for A_{1g} peaks the predicted frequency shifts have the same form for both proposed point groups (see Sec. III), these values cannot be used to make a choice between the two types of proposed structures.

B. E_{2g} peaks

Again, two of the strongest lines in the configurations which allow E_{2g} peaks (see Table II) were chosen for quantitative study. These are the lines located at 77.6 and 314.0 cm^{-1} at 77 K (see Table IV). Peak positions versus applied stress are plotted in Fig. 4. Here closed and open dots (squares) indicate frequencies of the α and β components of the E_{2g} representation (each a normal mode in the stressed crystal—see Sec. III), respectively, for $\hat{F}\|\hat{x}$ ($\hat{F}\|\hat{z}'$). Scattering configurations were chosen (using the polarizability tensors of Table II) so as to observe only one of the two components at a time. The configuration used in each case is indicated in Fig. 4. The solid lines are linear squares fits to the experimental points. From the slope of these lines and Eqs. (7) and (8), we obtain the deformation-potential constants a', b', c', and d' which are listed in Table V. If LaF_3 had the more symmetrical, D_{6h}^3, crystal structure the parameter d' obtained from this fit should be zero, within the experimental error, as discussed in Sec. III. The value of d' found for E_{2g} (78) is indeed very small and could be said to be zero within the experimental error. On the other hand, the E_{2g} (314) line exhibits a value of d' which, although small, is above the limits of experimental uncertainty. Hence the stress dependence of this line supports the less symmetric D_{3d}^4 structure. However, the value of d'/c' is, in absolute value, smaller than unity, lending support to the assumption that the deviations from the D_{6h}^3 structure are small.

C. E_{1g} peaks

In this case all but one ($\omega = 255.0$ cm^{-1}) of the E_{1g} structures observed in the zero-stress spectrum were sufficiently strong to allow quantitative evaluation of their behavior under stress. The greatest difficulty for quantitative analysis was encountered with the E_{1g} (299) line which is the weaker partner of a closely spaced doublet. Consequently, the points of peak position versus stress show their greatest dispersion here. The data are displayed in Figs. 5 and 6 following the same conventions described in Sec. IV B. Scattering configurations were chosen (using the polarizability tensors of Table II) so as to allow

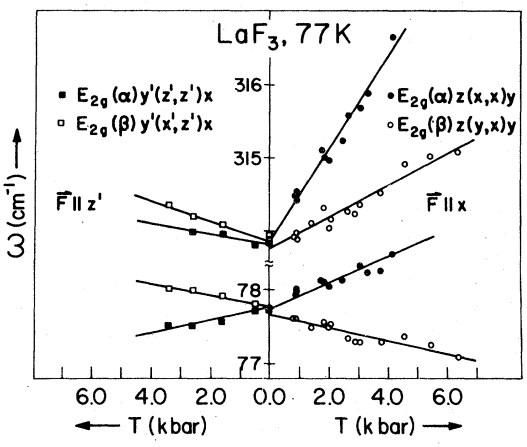

FIG. 4. Frequency vs stress for representative E_{2g} modes in LaF_3 for two directions of the applied force.

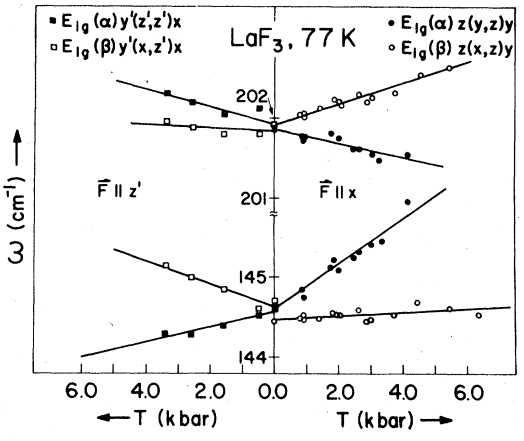

FIG. 5. Frequency vs stress for two E_{1g} modes of LaF_3 for $\hat{F}\|\hat{x}$ and $\hat{F}\|\hat{z}'$.

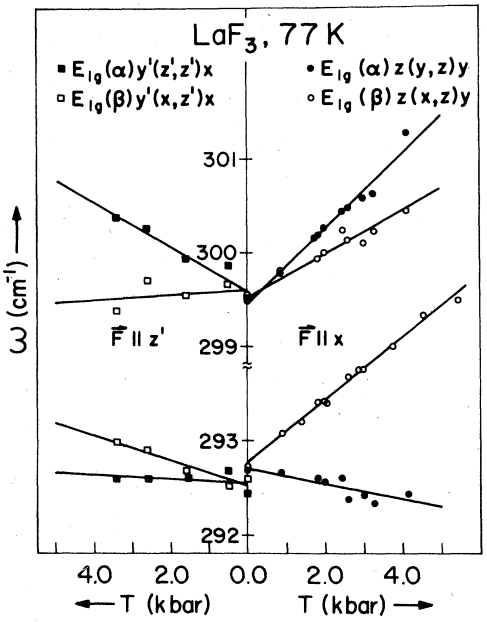

FIG. 6. Frequency vs stress for the doublet E_{1g} (293) and E_{1g} (299) for $\hat{F} \parallel \hat{z}'$.

the appearance of one of the two E_{1g} components at a time, and they are indicated in Figs. 5 and 6. Again, comparing the slopes of the frequency versus stress lines, obtained by a least-squares fit to the experimental data, with the results of Eqs. (7) and (8), we calculate the deformation-potential parameters a', b', c', and d' which are listed in Table V. As in the case of the E_{2g} lines, the coefficient d' should be zero, within the experimental error, if the structure of LaF_3 corresponded to the more symmetrical D_{6h}^3. This can be said to be the case only for the E_{1g} (202) line (see Table V). The E_{1g} (145) line has a value of d'/c' close to unity, while the remaining two lines, E_{1g} (293) and E_{1g} (299), have values of $|d'/c'|$ larger than unity. This gives unequivocal proof that the unit cell of LaF_3 has point-group symmetry D_{3d} rather than D_{6h}.

From the above discussion we see that from the behavior of the E_g lines under uniaxial stress we can draw definite conclusions as to which of the two proposed point-group symmetries, D_{6h} and D_{3d}, for LaF_3 is the true one. While the behavior of the E_{2g} (78) and E_{1g} (202) lines is compatible with either structure, that of the E_{1g} (145) and E_{2g} (314) strongly favors the structure whose unit cell has point-group symmetry D_{3d}. This conclusion is reinforced by the behavior of the E_{1g} (293) and E_{1g} (299) lines, whose deviations from predictions made on the basis of a D_{6h} point group are so large as to make it impossible to contemplate this possibility. Hence we conclude that the correct point-group symmetry of the LaF_3 unit cell is D_{3d}. That some peaks are more strongly affected by the deviations from the more symmetric structure than others is not surprising and argues in favor of the proposition of Bauman and Porto[11] that these deviations are not large. This conclusion is in agreement with the results from the Raman spectra of unstressed samples.

In conclusion, we have examined the zero-stress Raman spectrum of LaF_3 under conditions of extremely low temperatures and high resolution, identifying all the structures observed and correcting some inaccurate assignments in previously published data.[11] We examined the behavior of most of the Raman lines under uniaxial stress, obtaining numerical values for the anharmonic coefficients called deformation potentials.[16] Careful analysis of the stress data allows us to conclude that the correct point-group symmetry of the LaF_3 unit cell is D_{3d}.

ACKNOWLEDGMENTS

This work has been funded in part by Fundação de Amparo à Pesquisa do Estado de São Paulo and Conselno Nacional de Desenvolvimento Científico e Tecnologico.

[1]I. Oftedal, Z. Phys. Chem. B 5, 272 (1929); 13, 190 (1931).
[2]J. H. Van Vleck and M. H. Hebb, Phys. Rev. 46, 17 (1934).
[3]K. Schlyter, Ark. Kemi 5, 73 (1953).
[4]E. V. Sayre and S. Freed, J. Chem. Phys. 23, 2066 (1955).
[5]D. A. Jones, J. M. Baker, and D. F. D. Pope, Proc. Phys. Soc. (Lond.) 74, 249 (1959).
[6]J. M. Baker and R. S. Rubins, Proc. Phys. Soc. (Lond.) 78, 1353 (1961).
[7]E. Y. Wong, O. M. Stafsudd, and D. R. Johnston Phys. Rev. 131, 990 (1963); J. Chem. Phys. 39, 786 (1963).
[8]W. F. Krupke and J. B. Gruber, J. Chem. Phys. 39, 1024 (1963).
[9]M. Mansmann Z. Anorg. Allgem. Chem. 331, 98 (1964); Kristallografiya 122, 375 (1965).
[10]A. Zolkin, D. H. Templeton, and T. E. Hopkins, Inorg. Chem. 5, 1466 (1966).
[11]R. P. Bauman and S. P. S. Porto, Phys. Rev. 161, 842 (1967).
[12]V. Lemos, R. S. Katiyar, and F. Cerdeira, *Proceedings of the Sixth International Conference on Raman Spectroscopy, Bangalore, India, September 1978* (Heyden and Sons, Inc., London, 1978), p. 348.
[13]E. Anastassakis, A. Pinczuk, E. Burstein, F. H.

Pollack, and M. Cardona, Solid State Commun. 8, 133 (1970).
[14]F. Cerdeira, C. J. Buchenaver, F. H. Pollak, and M. Cardona, Phys. Rev. B 5, 580 (1972).
[15]S. Venugopalan and A. K. Ramdas, Phys. Rev. B 8, 717 (1973).
[16]V. J. Tekippe, A. K. Ramdas, and S. Rodriguez, Phys. Rev. B 8, 706 (1973).
[17]R. J. Briggs and A. K. Ramdas, Phys. Rev. B 13, 5518 (1976); 16, 3815 (1977).
[18]V. Lemos, F. Cerdeira, M. A. F. Scarparo, and R. S. Katiyar, Phys. Rev. B 16, 5560 (1977).
[19]OPTOVAC, Inc. North Broohfield, Mass.
[20]H. Vogelmann and T. A. Fjeldly, Rev. Sci. Instrum. 45, 309 (1974).
[21]T. C. Damen, S. P. S. Porto, and B. Tell, Phys. Rev. 142, 570 (1966).
[22]The notation used in this paper for point groups and their irreducible representations follows E. B. Wilson, Jr., J. C. Decius, and P. C. Cross, *Molecular Vibrations* (McGraw-Hill, New York, 1955).
[23]J. F. Nye, *Physical Properties of Crystals* (Oxford University, London, 1972).